Boundary-Layer Meteorol (2015) 155:229–248
DOI 10.1007/s10546-014-9999-y

ARTICLE

Footprint Estimation for Multi-Layered Sources and Sinks Inside Canopies in Open and Protected Environments

Tomer Duman · Josef Tanny · Uri Dicken · Mario B. Siqueira · Gabriel G. Katul

Received: 7 June 2014 / Accepted: 29 December 2014 / Published online: 10 January 2015

Abstract A multi-layered flux footprint model is developed for a canopy situated within a protected environment such as a screenhouse. The model accounts for the vertically distributed sources and sinks within the canopy as well as modifications introduced by the screen on the flow field and micro-environment. The effect of the screen on fetch as a function of its relative height above the canopy is then studied and compared to the case where the screen is absent. It is found that the required fetch is not appreciably affected by the vertical source–sink distribution in open and protected environments, but changes with the canopy density. Moreover, the fetch-to-height ratio is increased by the presence of the screen, at least when compared to the open environment case. How footprint analysis can be employed to estimate the ratio between above-canopy measured flux and vertically-integrated canopy source–sink strengths in a prototypical screenhouse is illustrated and further evaluated against eddy-covariance measurements from two screenhouse experiments.

Keywords Canopy turbulence · Flux footprint · Lagrangian stochastic model · Screenhouse

T. Duman (✉)
Nicholas School of the Environment, Duke University, Durham, NC, USA
e-mail: tomer.duman@duke.edu

J. Tanny
Institute of Soil, Water and Environmental Sciences, Agricultural Research Organization, Volcani Center, Bet Dagan, Israel

U. Dicken
Environmental Sciences and Energy Research, Weizmann Institute of Science, Rehovot, Israel

M. B. Siqueira
Department of Mechanical Engineering, Universidade de Brasilia, Brasília, Brazil

G. G. Katul
Nicholas School of the Environment & Department of Civil and Environmental Engineering, Duke University, Durham, NC, USA

1 Introduction

Assessing the spatial representativeness of eddy-covariance (EC) measured turbulent fluxes for biologically-active scalars above or within canopies continues to draw attention (Rannik et al. 2012). This assessment is now receiving renewed interest due to the proliferation of large-scale screenhouses where EC flux measurements of water vapour and CO_2 are proposed for irrigation scheduling (Tanny 2013). Current interpretation of flux footprint is essentially borrowed from open environments, where it is defined as a source weight function that describes contributions from all upwind surface emissions to a measured flux at some height above the surface (Leclerc and Thurtell 1990; Horst and Weil 1992; Hsieh et al. 2000; Schmid 2002; Vesala et al. 2008; Rannik et al. 2012). Footprint models commonly assume homogeneous surface sources positioned near ground-level or some effective displacement height, and further treat the bulk flow statistics as one-dimensional analogous to those above rough boundary layers with thermal stratification. These models have been incorporated into EC analysis software packages to assist in linking expected planar source area to EC measurement at the instrument height (Vesala et al. 2004). Specifically, these models provide the so-called 'effective fetch' (Pasquill 1972), which is the dynamic source area that is sensed by an EC sensor, and which now replaces the 100:1 fetch-to-height ratio rule-of-thumb previously used in many experimental designs (Leclerc and Thurtell 1990; Vesala et al. 2004, 2008).

Since their infancy in the early 1980s (Wilson et al. 1981), these methods have been extended to inhomogeneous surfaces and sources in the atmospheric boundary layer (ABL), where thermal stratification effects can be large (Leclerc and Thurtell 1990; Hsieh et al. 1997, 2000; Schmid 2002; Rannik et al. 2012). The framework for these extensions has been based on Lagrangian stochastic (LS) approaches, shown to be capable of accounting for realistic field conditions. However, studies that treat flux footprints in the context of complex canopy flows and vertically-inhomogeneous sources and sinks within the roughness or canopy sublayer (where most EC measurements are performed above tall forested ecosystems) are relatively scarce. Throughout, the terms roughness sublayer and canopy sublayer are used interchangeably because the canopy constitutes the main momentum absorbing roughness elements. Applying footprint analysis to EC measurements within agricultural structures such as a screenhouse, which is the main focus of this work, is further complicated by the presence of a screen. Not only does the addition of a screen alter the flow field and the canopy micro-climate, it also necessitates conducting EC measurements near the canopy top within a highly-disturbed canopy sublayer.

The effects of the vegetation on the footprint in open environments as influenced by modifications to the turbulent flow field due to the presence of the canopy have been considered, but many such calculations include only surface sources, which are either located at ground level or elevated above-ground (Baldocchi 1997; Hsieh et al. 2000; Lee 2003; Rannik et al. 2003; Mao et al. 2008; Prabha et al. 2008). The influence of source-strength distribution with height within the canopy volume has been considered in a limited number of studies (Rannik et al. 2000; Hsieh et al. 2003; Markkanen et al. 2003; Sogachev and Lloyd 2004; Sogachev et al. 2005). The canopy itself acts as a biologically active source of CO_2 and H_2O, therefore including vertically-distributed sources should be an inherent part of a canopy footprint model. For CO_2 the sign of the source becomes significant (positive for an emitting source and negative for a sink), since the vegetation acts both as a source and a sink for CO_2, respiring and photosynthesizing at different levels and at different times of the day. Methods for calculating the footprint for horizontally-heterogeneous sources and sinks are available (e.g. Sogachev and Lloyd 2004). However, no clear method has been provided for footprint

estimation of vertically-distributed sources and sinks, specifically for the case when both sources and sinks are active at the same time within the canopy volume.

The study objectives are two-fold: the first is to explore the effects of a canopy (without a screen) on footprint, taking into account not only the effects of canopy flow characteristics, but also investigating the influence of the vertical source–sink distribution within the canopy volume as representing the diurnal variation. The second objective is to understand how EC flux measurements in a screenhouse can be interpreted by footprint analysis. Three complications arise in such a set-up: (1) the limited space within such environments requires that the flux measurements be conducted in the canopy sublayer, which means that the vertical variation of scalar sources becomes significant; (2) the presence of the screen modifies the flow field and concomitant micro-environment (aerodynamic and radiative) in complex ways, which makes footprint modelling a challenge; and (3) the limited horizontal distance to the edge of the partially-enclosed structure complicates the relation between the source and the measured flux, since fetch requirements are less likely to be fulfilled. Both objectives are investigated here via a LS footprint model that includes diurnal variations of the source–sink distribution within the canopy volume. The effects of a screenhouse on the interpretation of EC flux measurements are then illustrated and further evaluated by comparing model calculations with EC measurements from two screenhouse experiments.

2 The Footprint Model

The LS footprint model includes three components: obtaining the Eulerian flow field and source–sink vertical distribution, calculating Lagrangian trajectories, and finally calculating the footprint function based on these trajectories. The flow-field model that was chosen here is described elsewhere (Siqueira et al. 2012) and the specific input of the cases that are considered here are addressed in Sect. 3. Here we deal with the other model components, specifically the details that are relevant to the calculation of the footprint of vertically-distributed sources and sinks.

2.1 The Lagrangian Stochastic Model

A conventional LS model is used here to calculate the flux footprint. In this model, N 'scalar' parcels are released from a source and their trajectories are computed by solving the generalized Langevin system of equations for the parcel velocity and position (Thomson 1987; Rodean 1996),

$$\mathrm{d}u_{pi} = a_i \mathrm{d}t + \sqrt{C_0 \epsilon}\, \mathrm{d}\mathbb{W}_i, \tag{1}$$

$$\mathrm{d}x_{pi} = \left(u_{pi} + \overline{u}_i\right) \mathrm{d}t, \tag{2}$$

where x_{pi} and u_{pi} are the parcel's position and turbulent velocity fluctuation, respectively; $\overline{u}_i$ and ϵ are determined from the fluid's Eulerian mean velocity and TKE dissipation rate at a given x_i. The constant C_0 is the Lagrangian Kolmogorov constant taken to be 3.125 based on a matching of the Lagrangian time scale to similarity theory (Li and Taylor 2005). The coordinates $x_1 = x, x_2 = y, x_3 = z$ are aligned so that x_1 is along the longitudinal or mean wind direction, x_2 is the lateral direction, and x_3 is the vertical direction. The velocity components $u_1 = u, u_2 = v, u_3 = w$ are aligned along x, y, z, respectively. The term $\mathrm{d}\mathbb{W}$ is the Wiener increment that constitutes the random component of the Langevin equation and is conventionally modelled by a zero mean Gaussian process with variance $\mathrm{d}t$, while the deterministic part a_i is as specified by Thomson (1987) to satisfy the well-mixed condition.

It should be noted that, while the model of Thomson (1987) satisfies the well-mixed condition, it is not a unique formulation. Several other schemes that satisfy the well-mixed condition have been suggested (e.g. Borgas et al. 1997; Wilson and Flesch 1997; Reynolds 1998a, b), but none of them was shown to be preferred over Thomson's model (Sawford 1999; Kurbanmuradov and Sabelfeld 2000; Hsieh and Katul 2009), which is adopted here. Although the dispersion model is not restricted to any source type and can accommodate point, line, or surface area sources, it is assumed here that the scalar source (or sink) originating from the canopy is sufficiently extended in the cross-wind direction (y). Therefore, the trajectory and velocity calculations, and later the footprint model, are inherently two-dimensional and the drift terms in the x and z directions simplify to

$$a_u = -\frac{C_0\epsilon}{A}\left(\sigma_w^2 u_\mathrm{p} - \overline{u'w'}w_\mathrm{p}\right) + \frac{1}{2}\frac{\partial \overline{u'w'}}{\partial z} + \frac{1}{A}\left[\sigma_w^2 \frac{\partial \sigma_u^2}{\partial z} u_\mathrm{p} w_\mathrm{p} - \overline{u'w'}\frac{\partial \sigma_u^2}{\partial z} w_\mathrm{p}^2 - \overline{u'w'}\frac{\partial \overline{u'w'}}{\partial z} u_\mathrm{p} w_\mathrm{p} + \sigma_u^2 \frac{\partial \overline{u'w'}}{\partial z} w_\mathrm{p}^2\right], \quad (3)$$

$$a_w = -\frac{C_0\epsilon}{A}\left(\sigma_u^2 w_\mathrm{p} - \overline{u'w'}u_\mathrm{p}\right) + \frac{1}{2}\frac{\partial \sigma_w^2}{\partial z} + \frac{1}{A}\left[\sigma_w^2 \frac{\partial \overline{u'w'}}{\partial z} u_\mathrm{p} w_\mathrm{p} - \overline{u'w'}\frac{\partial \overline{u'w'}}{\partial z} w_\mathrm{p}^2 - \overline{u'w'}\frac{\partial \sigma_w^2}{\partial z} u_\mathrm{p} w_\mathrm{p} + \sigma_u^2 \frac{\partial \sigma_w^2}{\partial z} w_\mathrm{p}^2\right], \quad (4)$$

$$A = 2\left(\sigma_u^2\sigma_w^2 - \overline{u'w'}^2\right), \quad (5)$$

where σ_u, σ_w are the Eulerian velocity standard deviations in the horizontal and vertical directions (x and z), and $\overline{u'w'}$ is the Reynolds stress, all of which are assumed to be known either through direct measurements or model calculations.

When a parcel crosses the EC sensor height (z_m), its crossing velocity (W) is stored along with the distance of the crossing location from its source, denoted as the fetch (X). A reflection scheme is applied at the ground, bouncing back each parcel position that arrives at the ground and reversing its vertical velocity component. Given a homogeneous infinite source in x, the inverted plume assumption (Pasquill 1971) may also be applied. This assumption states that, instead of releasing parcels from an infinite source, an equivalent footprint function can be calculated by releasing parcels from a point source and gathering all the information about multiple crossings at the sensor height (z_m) for each trajectory. This approach significantly reduces the computational costs since all the released parcels contribute to the footprint calculation at z_m. After storing all the crossing velocities and fetches, the footprint function can be evaluated.

2.2 Footprint Function Calculation for a Ground Source

The classical footprint function for a ground source has been extensively studied (Schmid 2002) and its calculation with the LS model is straightforward (e.g. Steinfeld et al. 2008; Vesala et al. 2008; Hsieh and Katul 2009). It is based on the equation

$$f(x) = \frac{1}{N\Delta x}\sum_{j=1}^{N}\sum_{k=1}^{n^j}\frac{W^{jk}}{\left|W^{jk}\right|} I\left(X^{jk}\right), \quad (6)$$

where N is the number of trajectories (set to the number of released parcels), and n^j denotes the total number of intersections of parcel j with the sensor height z_m. The indicator function I is unity for a fetch $(x - \Delta x/2) < X < (x + \Delta x/2)$ and zero otherwise. Only crossing velocities with a fetch that is within that grid cell contribute to the flux footprint at that x location. Each upward intersection with z_m is counted as a positive addition to the footprint by setting $W/|W| = 1$, and vice versa, a downward intersection is a negative addition $W/|W| = -1$. The cumulative flux footprint $F(x) = \int_0^x f(s)\mathrm{d}s \to 1$ by construction as $x \to \infty$, since each parcel that is released from the source is expected to reside above z_m as $x \to \infty$ when z_m is not too high above the ground. Attaining an $x \to \infty$ is not possible in practice, and a pragmatic measure used is the distance from the sensor that contributes 90 % of the total flux (termed X_{90}). This distance corresponds to x satisfying $F(x) = 0.9$. Other studies consider degraded fetch limits, such as X_{75} (e.g. Markkanen et al. 2003; Rannik et al. 2003), which are less strict. An error of more than 10 % in EC flux measurements due to mis-location of the sensor on top of other expected measurement errors is deemed too high. Moreover, it is shown later that X_{90} has low sensitivity to vertical source distribution. Another possibility of defining a required fetch may be based on the upwind x that achieves $|\mathrm{d}F(x)/\mathrm{d}x| \leq \delta$, where δ is sufficiently small. This fetch describes the distance from the source where $F(x)$ becomes constant rather than providing a specific contribution portion of the source to the measurement as does X_{90}. Although this definition might be deemed as useful for estimating an effective fetch in the roughness sublayer, the selection of δ remains ad hoc. Hence, to maintain a conventional definition and for comparisons with previous studies, X_{90} is used throughout unless otherwise stated.

2.3 Footprint Function Calculation for a Vertically-Distributed Source

For a vertically non-uniform source (but still infinite and homogeneous in x and y), such as in canopy flow where the entire canopy serves as a source (or sink) for biologically-active scalars such as CO_2 and water vapour, the total contribution of the sources and sinks to the flux that is measured by EC can be described as a 'weighted average' of multi-levels footprint functions. Each of these footprint functions $f(x, z_s)$ represents a different source release height (z_s). The computed $f(x, z_s)$ for each z_s is then weighted by the source–sink normalized distribution $Q(z_s)$ to construct a weight-averaged footprint function defined as,

$$f_{wa}(x) = \langle f(x, z_s) Q(z_s) \rangle. \tag{7}$$

The angled brackets represents vertical integration from $z = 0$ to h for any arbitrary quantity χ so that $\langle \chi \rangle = \int_0^h \chi(z)\mathrm{d}z$, where h is the top of the canopy, or more generally the highest location of a source (or sink) above the ground. The Q is defined as $Q(z_s) = q(z_s)/\langle |q(z_s)| \rangle$, where $q(z_s)$ is the amount (in mass or moles) of emitted scalar per unit time at a specific height z_s, and the source–sink distribution satisfies the normalizing property $\langle |Q(z_s)| \rangle = 1$. A cumulative flux footprint is now expressed as $F_{wa} = \int_0^x f_{wa}(s)\mathrm{d}s$.

Unlike a ground-source footprint, F_{wa} does not necessarily reach the value of 1 at a large fetch, as for the case of combined sources and sinks, and does not always monotonically increase with x. In such cases, X_{90} is not well-constrained (or unique) and should be re-defined, as discussed in Sect. 3.

3 Footprint Functions for a Canopy Flow in an Open Environment

3.1 Model Input

The LS model requires profiles of mean wind speed ($\overline{u}$), velocity variances (σ_u and σ_w), the Reynolds stress ($\overline{u'w'}$), and the TKE dissipation rate (ϵ). These canopy-flow statistics are computed here using a higher-order closure model, which solves the momentum balance equations for each of the Reynolds-stress terms, together with the continuity equation, and an additional equation for the TKE dissipation rate as described elsewhere (Siqueira et al. 2012). The solution of the flow depends on the friction velocity (u_*), the leaf area distribution shape with canopy height (LAD), as well as the leaf area index value ($LAI = \langle LAD \rangle$). Neutral conditions are assumed for illustration only, and model calculations were extended up to five times the canopy height. Various LAD profiles are used so as to compare canopies for which most of the foliage is concentrated at different heights (Fig. 1a). These profiles are described by a beta probability density function (i.e. $LAD(z) \sim (z/h)^{\alpha-1}(1-z/h)^{\beta-1}$, $z/h \in [0, 1]$), with shape parameters α and β (Markkanen et al. 2003) along with a normalizing constant to ensure that $LAI = \langle LAD \rangle$); LAI is varied between 1 and 4 so as to explore sparse and dense canopies, respectively. Figure 1 shows the flow statistics for several LAD and LAI combinations. The closure model for the flow has the ability to predict the typical characteristics of canopy velocity statistics, such as those found in field measurements (e.g. Finnigan 2000). The model is able to generate realistic TKE dissipation rate profiles with apparent peaks near the canopy top consistent with wind-tunnel and flume experiments described elsewhere (Poggi et al. 2008). All other model parameters and boundary conditions are identical to those used in Siqueira et al. (2012).

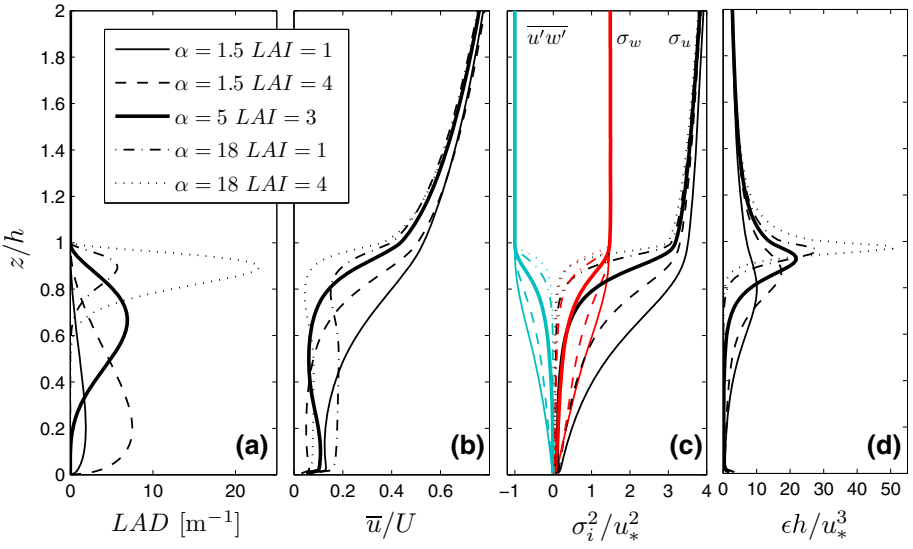

Fig. 1 The Eulerian flow statistics for five LAI and LAD combinations as computed by the second-order closure model. The LAD profiles are described by a beta probability density function. The shape parameter β is kept constant in all model runs ($\beta = 3$). The modelled mean wind speed is normalized by the velocity at the upper boundary ($U = \overline{u}(5h)$)

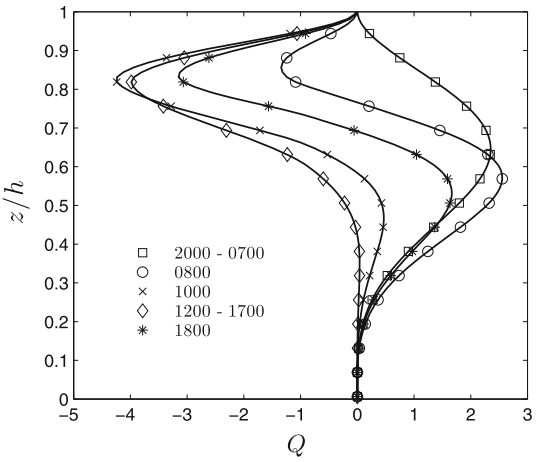

Fig. 2 CO_2 flux source–sink normalized distribution (Q) at different times of the day (local time), as computed by the transport model for the case of $\alpha = 5$ and $LAI = 3$ in the absence of soil respiration. Q satisfies the normalization $\int_0^h |Q|\,\mathrm{d}z = 1$

The source–sink distribution shape needed for the footprint estimation is now computed with a scalar transport model that solves simultaneously the transport equations for water vapour, CO_2, and air temperature (Siqueira et al. 2012). To describe the effect of diurnal variations on the flow and scalar transport, mean meteorological forcings were specified by changing the friction velocity, the shortwave radiation, the mean air temperature, and relative humidity during the day, similarly to the conditions described in Siqueira et al. (2012). This model considers the physiological as well as radiative properties of the vegetation, and is able to reproduce the diurnal cycle of the scalar source–sink distribution profile with z. A simplified case study is considered where the CO_2 source–sink profiles for a specific case ($\alpha = 5$ and $LAI = 3$) is shown in Fig. 2 at different times of the day in the absence of any soil respiration or storage (again for maximum simplicity). Even without soil respiration, two periods can be observed: a nocturnal period, where photosynthesis is suppressed and the entire above-ground vegetation biomass releases CO_2 through above-ground respiration; and during the high noon period (1200 to 1700 local time), where the entire canopy uptakes CO_2 due to photosynthetic activity. In between these times, there are 'transitional periods' during which the upper storey of the canopy still undergoes photosynthesis, but the lower part does not have sufficient sunlight and is dominated by respiration terms. The soil CO_2 can be added to these simulations if known, but is taken here as zero for illustration only.

In each of the LS calculations 2×10^6 particles were released with a uniform distribution from the ground to the canopy top. 20 virtual sensor heights were chosen, evenly spaced between $z_m = 0.1h$ to $2h$. For each trajectory all crossing velocities (W) and fetches (X) were stored at each sensor height. Using these results, for each sensor height 100 footprint functions were calculated according to Eq. 6 (with $N = 2 \times 10^4$) at 100 z_s locations evenly spaced within the canopy volume. These multi-levels footprint functions, $f(x, z_s)$, were later weight-averaged to determine f_{wa} according to Eq. 7.

3.2 The Influence of the Source Vertical Distribution on the Flux Footprint

The case of $\alpha = 5$ and $LAI = 3$ serves here as a reference to examine the sensitivity of the scalar flux footprint to the source–sink vertical distribution. Three computed CO_2 source–sink distributions within the vegetation system are considered as illustration, describing nighttime (only sources), daytime (only sinks) and transitional periods (combined sources and sinks).

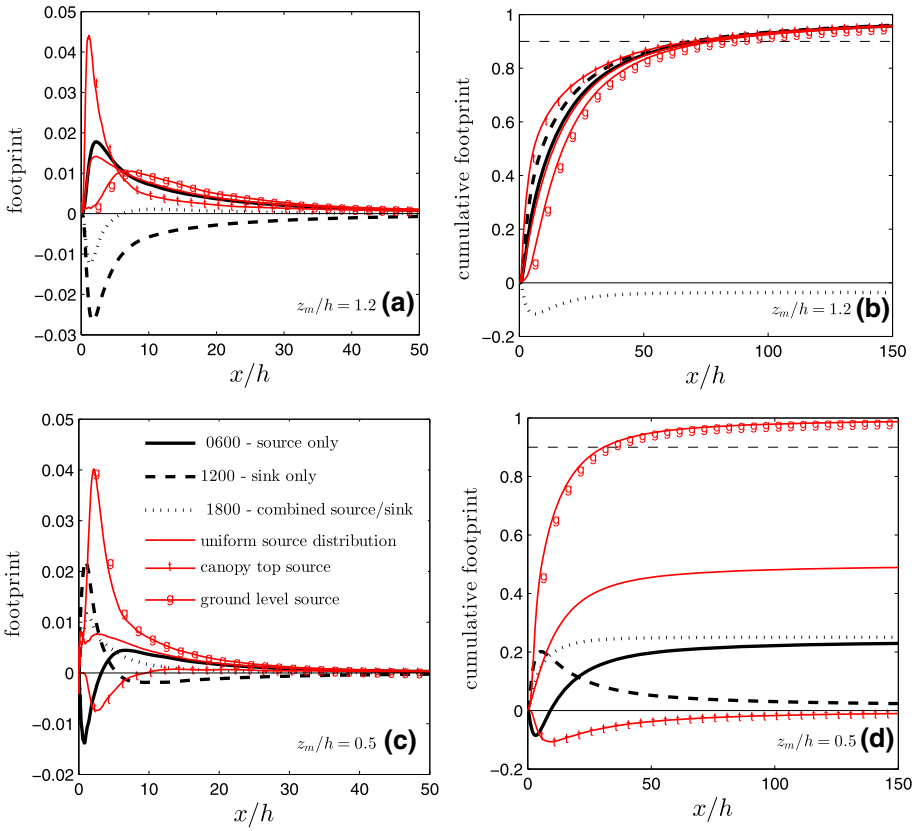

Fig. 3 Footprint predictions by the Lagrangian stochastic footprint model for the case of $\alpha = 5$ and $LAI = 3$. **a**, **b** show f_{wa} and F_{wa} for $z_m/h = 1.2$ respectively. **c**, **d** show the same for $z_m/h = 0.5$. The cumulative footprint of the sink-only case for $z_m/h = 1.2$ is purely negative, but presented here (in (**b**)) in positive values for convenience. A *solid horizontal line* marks the zero value, and the *dashed horizontal line* (in (**b**) and (**d**)) stands for $F_{\mathrm{wa}} = 0.9$

In addition, a height-uniform source, and a concentrated source either at the ground or at the canopy top were also considered for comparisons. Figure 3 shows the averaged footprint functions $f_{\mathrm{wa}}(x)$ and the cumulative footprint flux $F_{\mathrm{wa}}(x)$ for each of these six source–sink distributions at two measurement heights: a sensor above the canopy ($z_m/h = 1.2$) and a sensor that is located within the canopy ($z_m/h = 0.5$).

3.2.1 Above-Canopy Sensor: Pure Sources or Sinks

The footprint functions of an above-canopy sensor (Fig. 3a) that describe purely positive or negative sources (i.e. all cases except for the combined source/sink at 1800 local time) reveal a 'classical' footprint function shape with a peak value near the sensor and a slow decay further away upwind, and are similar to functions previously shown in Markkanen et al. (2003) and Sogachev and Lloyd (2004). The peak is closest to the sensor and has the largest value when the source is concentrated at the top of the canopy. When the source is placed near the ground, the peak is much further upwind from the sensor and the function is much

more spread as expected. For the cases of distributed pure source or sink (source only, sink only, and uniformly distributed source) the footprint functions are rather similar in spread, peak location, and peak value. These features are also reflected in the cumulative footprint (Fig. 3b). The canopy-top concentrated source accumulates the fastest, and the ground source accumulates the slowest. The cumulative footprints of the distributed source (or sink) cases reside between these two extremes and accumulate at a similar rate. In spite of differences between footprint functions, the cumulative footprint of all the five cases discussed here reach 0.9 at about the same distance from the sensor, which means that their X_{90} is similar.

3.2.2 Above-Canopy Sensor: Combined Sources and Sinks

The footprint function for the case of combined sources and sinks shows a different behaviour. Unlike the other footprint functions, it includes both positive and negative values (Fig. 3a). The region near the sensor contributes to a downward flux that is measured by the sensor, and at the same time larger fetches contribute to upward fluxes. In this case, the cumulative function does not saturate at unity, but to the integrated sources and sinks ($\langle Q \rangle$). It is to be noted that the measured flux is irrespective of the flow field, but the concentration is not, since the linkage between flux and concentration is dependent on the flow field. Here the integrated sink strength is slightly larger than the source strength (see Fig. 2), so the final value of the cumulative footprint is negative and small (-0.036). Although Markkanen et al. (2003) and Sogachev and Lloyd (2004) did not consider a case of a combined distributed sources and sinks, they studied a case of a canopy sink combined with a ground soil flux source. Their footprint functions show similar behaviour to the function presented here. The cumulative footprint does not monotonically saturate at a final value, but peaks near the sensor and then slowly decays with increasing distance. Therefore, an inadequate fetch might result in a measured flux that is larger than the actual source–sink flux. The shape of the cumulative footprint makes it difficult to determine X_{90} by solving for x satisfying the condition $F_{\mathrm{wa}}(x) = 0.9$. One way to delineate X_{90} is to choose the distance where the measured flux is 10 % larger than the net source (or sink) flux instead of 10 % smaller. Here, we choose to estimate X_{90} as a weighted average of all X_{90} values of each of the multi-level sources or sinks, which represents 90 % contribution of each level to the measured flux (whether it is a source or a sink). Fetch analysis is further discussed in Sect. 3.2.4.

3.2.3 Within-Canopy Sensor

Measuring fluxes in the understorey of a canopy (as is routinely done in forest-floor CO_2 efflux estimates), has the advantage of requiring a much smaller fetch, not only because the sensor is closer to the ground but also since the mean velocity within a canopy is reduced (roughly exponentially) with decreasing height. At the same time, a sensor that is located within a canopy only captures a fraction of the source flux.

Figure 3c and 3d presents the footprint functions and the cumulative footprint for a sensor that is located within the canopy ($z_m/h = 0.5$). The only case that shows a classical footprint function shape is the ground-level source, since the entire source is located below the sensor. It is also the only case for which the cumulative footprint saturates at unity, which means that for an infinite fetch the sensor 'sees' the entire source.

The case of a canopy-top concentrated source demonstrates the behaviour of a footprint function for a source that is located above the sensor. Here, every air parcel that crosses the

measurement height downwards is reflected from the ground and crosses z_m again in the opposite direction. Since the sensor height is always much smaller than the boundary-layer height, a released parcel is most likely to reside above z_m at large fetches. Therefore, if the source is horizontally infinite and homogenous in x and the fetch is large enough, the sensor should measure a zero flux. This can be seen by looking at the cumulative footprint for a canopy-top source at Fig. 3d: in the near-field a downward flux is detected, which after $x \approx 10h$ decays as a result of a counter-direction flux upward due to reflection from the ground, until F_{wa} reaches zero at large fetches.

For the cases of vertically distributed sources (or sinks), each source level that is located above the sensor has a zero contribution to the measured flux. Thus, the flux that is 'seen' by the sensor is the integrated source distribution of only levels that are below the sensor: $F_{\mathrm{wa}}(z_m) \rightarrow \int_0^{z_m} Q(z)\mathrm{d}z$. For a uniformly distributed source, F_{wa} in Fig. 3d adds to exactly 0.5 since the sensor is exactly at mid-canopy, and therefore measures only half of the total source. For the realistic source–sink distributions (that were generated by the transport model), the final value of the cumulative footprint corresponds to the integrated source strength up to $0.5h$, which is different for each of the cases.

The cumulative footprint can be used to assess the likely measured flux as a function of the available fetch upwind from the sensor. On the other hand, estimation of X_{90} for a sensor that is located within the canopy usually cannot be achieved with the cumulative footprint due to its complex shape. Since the levels above the sensor do not contribute to the measured flux, X_{90} was computed by accounting only for sources (or sinks) that are located below the sensor height. Therefore, X_{90} is calculated here as the weighted average of all X_{90} values of the multi-level sources or sinks located below the sensor.

3.2.4 Effective Fetch Analysis

Figure 4 shows how X_{90} varies with measurement height for each of the six cases of source–sink distributions. Despite the differences in the footprint functions, and although at different times of the day the measured flux by the sensor varies considerably, the differences between the profiles of X_{90} are small both within the canopy and above it. This can be explained by the fact that no matter where the source is located or how it is distributed with height, the air parcels sample the entire flow profile within the canopy due to the reflection at the ground. It is

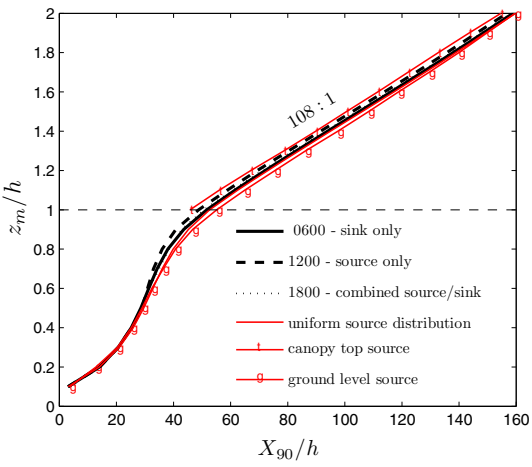

Fig. 4 The variation of X_{90} with measurement height for six source–sink distributions. The results are for the case of $\alpha = 5$ and $LAI = 3$

to be noted that Sogachev and Lloyd (2004) reported a much larger difference in X_{90} of $\approx 20h$ between a ground source and a canopy-top source for the case of a denser canopy ($LAI = 5.6$ with foliage concentrated at the top half of the canopy). However, even when checking such a case, it exhibited $\approx 70\,\%$ less variability in X_{90} for realistic source distributions, such as those shown in Fig. 2, compared with the extreme ground and canopy-top source cases. Rannik et al. (2012) also considered a CO_2 vertically distributed sink profile, and although only one sink profile was used in their work, they also found that the footprint is not very sensitive to the shape of the profile.

Although the sensitivity of X_{90} to the source distribution is weak (especially for realistic source–sink distributions), it is much more sensitive to the normalized sensor-height location. This is most pronounced above the canopy, where X_{90} grows rapidly with height and has an approximate linear trend. For the case presented here, the fetch-to-height ratio is 108:1, which means that an elevation of the flux sensor in 1 m increases the fetch by 108 m. This linear behaviour is similar to that found in classical boundary-layer flows, but with a much lower fetch-to-height ratio. For a similar LS model run for a neutral ABL case, the fetch-to-height ratio was about 240:1, which is much higher than the 100:1 rule-of-thumb known to underestimate the required fetch needed upwind of the sensor (Leclerc and Thurtell 1990).

The shape of X_{90} as a function of sensor height can be linked with the mean wind speed and with the *LAD* profile (Fig. 1). For the canopy shown here ($\alpha = 5$ and $LAI = 3$), the leaf density is low near the ground and the wind speed is relatively high, therefore X_{90} expands rapidly with height. Most of the foliage is concentrated in the upper half of the canopy where the wind speed is reduced and therefore X_{90} in this section grows less rapidly with increasing height.

The insensitivity of X_{90} to the source (or source–sink) distribution was found to be consistent for the entire range of *LAI* and *LAD* that were tested here (not shown). It can be surmised that, although the vertical distribution of sources and sinks change during the day, the required fetch necessary to measure 90 % of the flux for a sensor located at a specific height z_m is robust to such changes (for neutral conditions and realistic source–sink distributions).

3.3 The Influence of the Leaf Area Density on the Footprint

While X_{90} was shown to be uninfluenced by the precise shape of the source–sink distribution, it is dependent on the velocity profile and the other flow statistics, which change with values of *LAI* and *LAD*. Figure 5 shows the X_{90} profiles for four extreme cases that represent combinations of high and low values of *LAI* with high and low values of the beta distribution parameter α (describing a canopy that is denser in its lower part and higher part respectively, as shown in Fig. 1). It is to be noted that neither the footprint functions nor the X_{90} profiles are dependent on the value of the friction velocity (u_*) or the canopy height (h), since the model is perfectly scaled with these two parameters in near-neutral flows. Therefore not the absolute values of flow statistics but their normalized profiles affect the differences in X_{90} shown in Fig. 5.

In Fig. 5, two opposite behaviours can be delineated within the canopy. For a canopy that is dense in its lower part ($\alpha = 1.5$), the fetch increases slowly until $z_m \approx 0.6h$ and then more rapidly in the upper sparse canopy section. For $\alpha = 18$, the fetch increases rapidly in the lower low-density part and then its growth rate decays in the upper dense-canopy part. Therefore, the *LAD* distribution affects the rate that X_{90} increases with height within the canopy. In regions of low vegetation density, the increase of the fetch with height is rapid, and vice versa. Increasing *LAI* reduces X_{90} within the canopy primarily through a reduction in the relative wind speed caused by total drag effects (Fig. 1b).

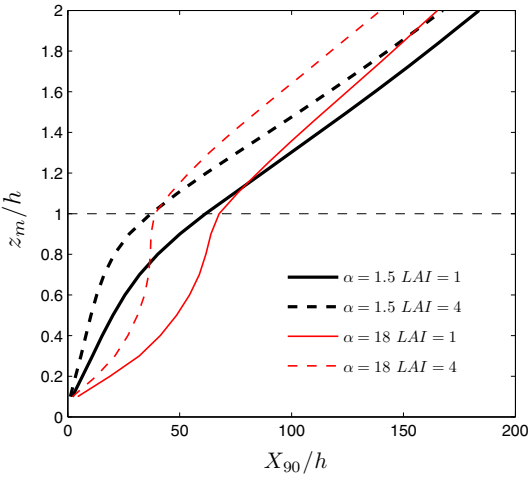

Fig. 5 The variation of X_{90} with measurement height for the combinations of high and low values of *LAI* with high and low values of the beta distribution parameter α

Above the canopy, the fetch-to-height ratio is constant for all cases, and is not affected by *LAI* variations. Changing *LAD* distributions within the canopy does affect this ratio above the canopy. For $\alpha = 18$, the ratio is 1.3 times smaller than for $\alpha = 1.5$ (92:1 vs. 122:1).

4 Footprint for Screenhouse Protected Canopy

The LS model is now used to develop guidelines for EC sensor placement in protected environments such as screenhouses. EC flux measurements in large screenhouses were reported by several authors (Möller et al. 2004; Tanny et al. 2006, 2010; Dicken et al. 2013), but the interpretation of such EC measurements remains in its infancy. The addition of a screen requires modification to the flow and scalar transport models, and hence, is expected to alter the fetch requirements.

4.1 The Effect of the Screen on the Effective Fetch

The effects of the screen on the flow are considered using an additional drag-force element with a non-isotropic drag coefficient and a drag dissipation term. This additional screen-induced drag force is locally placed at the screen height (h_{sc}) and has a formulation similar to the canopy-drag effect. Furthermore, the screen acts as a source–sink for sensible heat, necessitating a full energy balance calculation for the screen temperature. The screen also modulates the incoming radiation by shading and this modulation depends on the screen properties and incident radiation beam angle. In practice, growers deploy screens at different heights above the canopy, and the screen-height to canopy-height ratio (h_{sc}/h) may also affect the flow and the transport properties. All these effects are incorporated into the flow and scalar transport models, as they have direct bearing on the flow field and source–sink scalar distribution within the protected canopy. The flow and transport-model formulations and the effect of the screen on the mass, momentum, and energy exchange rates are described elsewhere and are not repeated here (Siqueira et al. 2012). Only the effect of the screen on the footprint-model results is presented.

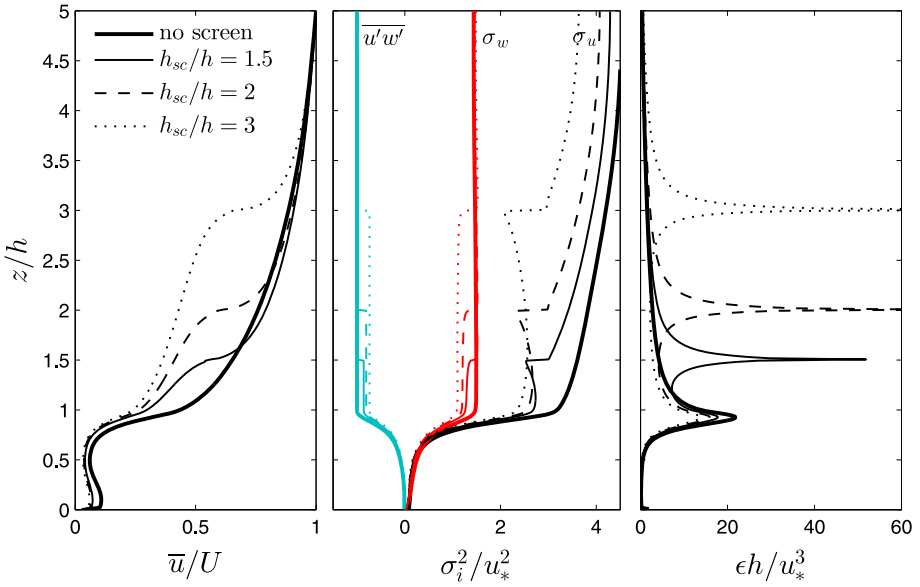

Fig. 6 Flow statistics with and without a screen for three screen-height to canopy-height ratios. The results are presented for the case of $\alpha = 5$ and $LAI = 3$ ($C_{\mathrm{d,sc}} = 0.02$)

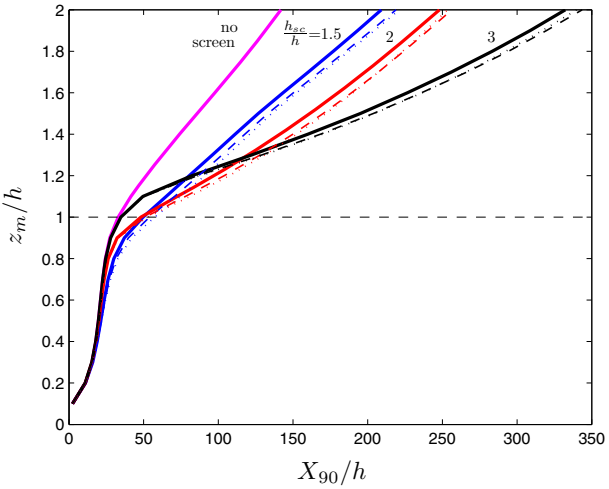

Fig. 7 The variation of X_{90} with measurement height with and without a screen for three screen-height to canopy-height ratios. The results are presented for the case of $\alpha = 5$ and $LAI = 3$. The effect of screen drag coefficient variation is marked by a *solid line* for $C_{\mathrm{d,sc}} = 0.02$, *dashed line* for $C_{\mathrm{d,sc}} = 0.04$, and *dotted line* for $C_{\mathrm{d,sc}} = 0.08$

Figure 6 shows the flow statistics for three h_{sc}/h values as well as for a no-screen case, and Fig. 7 shows X_{90} profiles as a function of sensor height for the same cases. X_{90} profiles were tested and were found to be insensitive to the source–sink variation with height even when the screen is added. Thus, Fig. 7 was generated with a height-uniform distributed scalar source. The addition of the screen increases X_{90}, mostly above the canopy. The fetch-to-height ratio

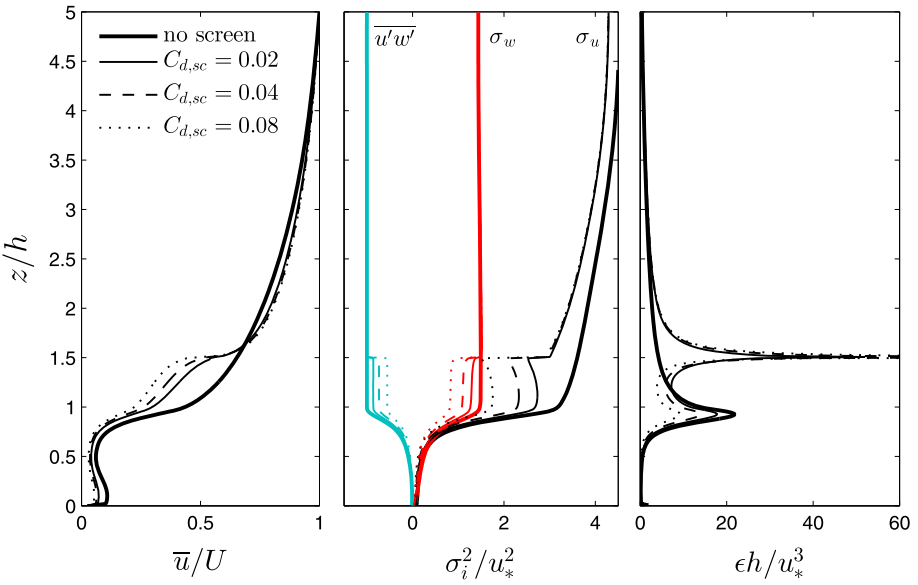

Fig. 8 Flow statistics with and without a screen for three screen drag coefficients. The results are presented for the case $\alpha = 5$ and $LAI = 3$, with $h_{sc}/h = 1.5$

above the canopy increases with h_{sc}/h (often due to a reduced h at the early phases of crop development). Since the normalized profiles of the flow statistics are those that affect the differences in X_{90} and not the absolute values, the increase in the required fetch when adding the screen may be explained by the relative reduction in the mean velocity magnitude (primarily) at the screen height. It is evident from Fig. 6 that the higher the screen is relative to the canopy top, the portion of height where the velocity is reduced becomes larger. Although the largest changes in all the flow statistics occur at the screen height, including the Reynolds stresses and TKE, no drastic changes in X_{90} can be delineated at this specific height, as shown in Fig. 7 for $h_{sc}/h = 1.5$ and 2. This finding can be explained by the fact that, (1) the screen acts as a localized drag element, unlike the canopy, and is also pervious to gas exchange (i.e. parcels can move up and down through the screen), and (2) the screen is above z_m whereas the footprint is sensitive to the flow field and source strength below z_m as previously shown in the open environment. It is to be noted here that, while the screen is pervious to mass exchange, it can act as a source (or sink) for heat. Hence, many of the earlier findings do not hold for air temperature, where the heat source (or sink) originating at the screen must be accommodated in the footprint analysis through Q (as before).

In addition to the effect of screen height, the effect of aerodynamic screen resistance on the footprint was tested by altering the screen drag coefficient ($C_{d,sc}$). A higher $C_{d,sc}$ represents a denser screen mesh as may be needed against insect invasion. Figure 8 presents the flow statistics that were computed with three different values of $C_{d,sc}$ for the case of $h_{sc}/h = 1.5$ ($C_{d,sc} = 0.02$, 0.04, and 0.08). As expected, enlarging the drag considerably influences the Reynolds stress and the velocity standard deviation profiles. However, the relative mean velocity is mildly affected by the change of $C_{d,sc}$. Figure 7 presents the effect of the variation of the screen drag for each of the X_{90} profiles (solid line for $C_{d,sc} = 0.02$, dashed line for $C_{d,sc} = 0.04$, and dotted line for $C_{d,sc} = 0.08$). The screen drag shows only a small effect on the required fetch, which may be explained by the small effect of $C_{d,sc}$ on the mean velocity.

Table 1 Modelled fetch-to-canopy-height ratio and X_{90} values for three different stages of a plant's growth cycle within a screenhouse

h_{sc}/h	h (m)	z_m/h	X_{90}/h	X_{90} (m)	$F_m/F_s\|_{d=100\,m}$	$F_m/F_s\|_{d=150\,m}$
3	2	2.5	434 (212)	868	0.38	0.47
2	3	1.66	192 (124)	576	0.58	0.62
1.5	4	1.25	85 (78)	340	0.64	0.74

$h_{sc} = 6$ m, $z_m = 5$ m, $\alpha = 5$ and $LAI = 3$. Values of fetch-to-height ratio for a no-screen case are added in parenthesis for comparison. Also presented are the modelled flux fraction F_m/F_s when the upwind distance to the edge of the screen is $d = 100$ m and $d = 150$ m, for a case of a nocturnal source distribution shown in Fig. 2 (2000–0700 local time), assuming no contribution of the fluxes from outside of the screenhouse

This result also explains the high dependency of the footprint on the mean velocity, rather than on the other higher-order flow statistics.

4.2 Application to EC Flux Measurement Interpretation

When an EC flux-measurement system is placed within a screenhouse, EC sensors must be located far enough from edges to ensure that the measured flux converges to the vertically-intgrated sources and sinks. The recommended distance could be X_{90} that is calculated by the footprint model. From Fig. 7, the screen adds a disadvantage over an open vegetation scenario, since it enlarges the fetch-to-height ratio and therefore requires a larger distance from the edge to measure 90 % of the source–sink profile. This is especially problematic for a limited-sized screenhouse structure. However, vegetation height inside a screenhouse is commonly no more than a few metres. Hence, the fetch requirement is much lower when compared with forested canopies (in absolute distances). Moreover, for an existing screenhouse structure h_{sc} is constant, but h_{sc}/h may evolve depending on crop development and harvest time. Therefore, for low vegetation (high h_{sc}/h) the X_{90}/h value might be large, but the actual distance that is needed for a 90 % fetch may not be much larger than for tall vegetation. As an example, Table 1 presents the values of X_{90} for three different plant heights within a 6 m high screenhouse, and with a sensor that is located at $z_m = 5$ m, as computed by the footprint model.

As the canopy grows from $h = 2$ to 4 m, X_{90}/h becomes ≈5 times smaller. However, the actual size of X_{90} is only ≈2.5 times smaller. Still, these required fetches are relatively large and cannot be readily achieved in many operational screenhouses. Given the distance of the sensor from the edge of the structure (d), the footprint model can be used to estimate the fraction of the source flux that is measured by the sensor inside the protected environment, provided fluxes from the outside are known. This is done by computing the value of the cumulative footprint function at the desired fetch ($F_m = \int_0^d F_{wa}(s)\mathrm{d}s$). For example, Table 1 includes the modelled ratio of measured flux to source flux (F_m/F_s, where $F_s = \langle Q \rangle$) when the upwind distance to the edge of the screen is $d = 100$ and 150 m for the case of positive sources only, assuming that the contribution of the fluxes from outside of the screenhouse is negligible. As expected from previous results, although the height of the sensor is kept constant, the fraction of the source flux that is 'seen' by the sensor increases considerably when the vegetation grows and the sensor becomes closer to its top. Since the fetch requirements are not satisfied, the measured flux underestimates the source flux, and the model may be used to predict the needed correction.

Beyond the edge of the screenhouse structure, the physical conditions are different: it is assumed that there is no vegetation or screen and therefore the wind profiles are different, which should affect the footprint calculation. While the model is capable of accommodating this kind of horizontal flow inhomogeneity (without using the inverse plume assumption, but with a full forward scheme), the developing section of the flow is not yet understood for screenhouses. Here, it is assumed that the flow statistics rapidly adjust to the vegetation and the screen resistance. This assumption however might be fairly reasonable for an extensive screenhouse, due to the existence of the side screen walls and the relatively small gap between the canopy and the top screen that should dampen the momentum adjustment in a short distance from the edge of the structure. Ignoring the higher velocity at the entrance to the screenhouse results in some overestimation of the required fetch by the model.

Validation of footprint models requires complex experiments. Only a handful of such validations are available, which usually show promising abilities of the LS approach, as summarized in Rannik et al. (2012). Flux measurements in screenhouses are even more challenging. A previous study has already shown that EC measurements can be utilized in such an environment (Möller et al. 2004; Tanny et al. 2006, 2010; Dicken et al. 2013). One way of using EC measurements to validate a footprint model is by placing two sensors at two different heights within the screenhouse, both of them above the canopy. By comparing the ratio between the measured fluxes (F_{m1}/F_{m2}, where 1 and 2 stand for the lower and higher sensors respectively), the effect of a finite footprint can be tested. Although some EC measurements are available inside screenhouses, most previous experiments included only one sensor at one measurement height. Dicken (2011) conducted a measurement campaign during 2009 that included multiple locations where two EC sensors were positioned at two heights above a banana canopy. Only one set of measurements from this campaign was found suitable for model comparison, since it was the only set that showed a near-constant momentum flux above the canopy (see the constant Reynolds stress in the gap between the top of the canopy and the screen in Fig. 6). Such a constant Reynolds stress may be used to identify how close the flow field is to equilibration for the conditions inside the screenhouse. The experiment was conducted in the Carmel northern coastal plain in Israel within a large banana screenhouse (with dimensions of $200 \times 400 \times 6\,\mathrm{m}^3$). The canopy height during the measurements was $\approx 2\,\mathrm{m}$ and the two EC sensor systems were positioned at $z_{m1}/h = 1.1$ and $z_{m2}/h = 1.6$, with a vertical distance of 1 m between them. Another experiment was conducted during 2006 in a banana screenhouse ($230 \times 300 \times 6\,\mathrm{m}^3$) situated along the eastern coast of the Sea of Galilee (Lake Kinneret) in northern Israel (Tanny et al. 2010). Here, $h = 4$ m and the EC sensors were positioned at $z_{m1}/h = 1.19$ and $z_{m2}/h = 1.34$. For model calculations, LAD was assumed to have a beta distribution with $\alpha = 5$ and $LAI = 3$ in both campaigns, which are appropriate for banana plantations (Siqueira et al. 2012).

The modelled flux fraction F_m/F_s above the canopy for a reported minimum fetch of $d = 90$ and 110 m to the edge of the structure for the Carmel experiment and the Kinneret experiment respectively is shown in Fig. 9. The modelled curves show an approximate linear decrease of the flux with sensor height that is similar for the CO_2 sink flux and the water vapour source flux for a daytime source-distribution profile. The lower F_m/F_s values for the Kinneret experiment are a result of the lower sensor's proximity to the edge with respect to the canopy height, which is $d = 27.5h$ for this experiment compared to $d = 45h$ in the Carmel experiment. The modelled flux ratio F_{m1}/F_{m2} for the Carmel experiment was 1.22, which is close to the measured value of 1.26 for CO_2 and water vapour. The fact that the same flux ratio for CO_2 and water vapour was measured further demonstrates the low sensitivity of the footprint to the source distribution within the canopy (as previously discussed for the open-canopy case). For the Kinneret experiment, the modelled and measured ratios are 1.17 and

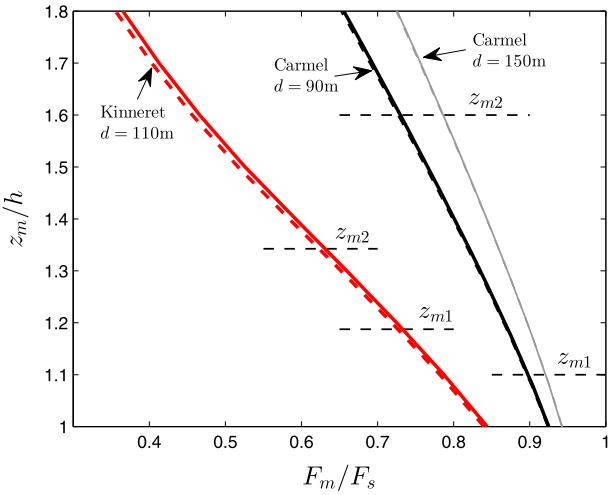

Fig. 9 The modelled flux fraction F_m/F_s above the canopy that correspond to EC measurements in two large banana screenhouses (the Carmel and Kinneret experiments). The model results are shown for an available fetch of $d = 110$ m to the edge of the structure in the Kinneret case, and for $d = 90$ and 150 m for the Carmel case. *Solid* and the *dashed lines* stand for CO_2 and water vapour fluxes, respectively. The heights of two EC sensors in the experimental set-up are marked by *horizontal dashed lines*, separately for each of the two experiments

1.23 respectively. The minor underestimation of the model in both cases might be explained by not taking into account the edge effects on the flow. The assumption of neutral stability may also affect the results, since most measurements were made during daytime, when the conditions are usually unstable. Although unstable conditions were shown to reduce the required fetch for ABL flows (Rannik et al. 2012), it is less expected to affect the footprint within the screenhouse where the momentum is controlled mostly by the presence of the screen.

Another issue that should be dealt with when estimating the flux ratio is the available fetch that changes over time with wind direction and affects the measured flux as a result. As an example, in the Carmel experiment a 90-m fetch was a minimum for purely northerly or southerly winds, while winds on the coastal plane in Israel are mostly southerly or north-westerly yielding higher fetch values. Since the flux ratios obtained ($F_{m1}/F_{m2} = 1.26$ for water vapour and CO_2) are for pooled data, without filtering wind directions, the results in Fig. 9 are shown also for an available fetch of $d = 150$ m. Increasing the fetch increases the measured flux at the lower sensor by only 2.3 %. The effect becomes more pronounced when the sensor is located at higher levels, showing a 5.6 % increase for the upper sensor, which is only 1 m higher.

The results that are shown in Fig. 9 can also be used to estimate a 'correction factor' for EC flux measurements assuming no sources and sinks for water vapour or CO_2 outside the screenhouse (mainly a near-desert environment). Based on model results, the fluxes measured by the lower and upper sensors for the Kinneret experiment are 73 and 62 % of the source flux respectively. A similar estimation can be found in Tanny et al. (2010) for the same experiment, applying the approximate analytical footprint model derived by Hsieh et al. (2000). While the modelled flux ratio is approximately the same ($F_{m1}/F_{m2} = 1.15$ for the semi-analytical solution versus 1.17 for the LS model presented here), the semi-analytical model does not

take into account the screen effects, and as anticipated from previous results overestimates the measured flux, predicting 84 % of the source flux for the lower sensor and 73 % for the upper sensor. These findings suggest that, despite the added computational costs of using the LS footprint model compared with an analytical model, this added cost may be necessary when dealing with complex flows such as those characterizing screenhouses.

5 Conclusions

A Lagrangian stochastic model has been used for footprint analysis of multi-layered sources and sinks inside canopies in open and protected environments. It is shown that the footprint for a combined source and sink distribution and the footprint for an in-canopy flux sensor do not conform to the conventional cumulative footprint shape, necessitating other considerations for estimating the effective fetch. An important finding from the footprint-model simulations here is that the recommended location of an EC flux sensor (in the form of X_{90}) appears robust to the precise shape of the source–sink distribution within the canopy. This finding is encouraging given that the source–sink distribution for biologically-active scalars varies appreciably in depth and time during the day. It is also shown how fetch requirements are altered with canopy density. The required fetch becomes smaller for higher values of *LAI* and for canopies that are denser in their upper region. This effect is visible not only when the sensor is located within the canopy, but also changes the fetch-to-height ratio above the canopy. This fetch-to-height ratio was found to be more than twice smaller than in a neutral ABL in the absence of a canopy. In protected environments such as screenhouses, the addition of a screen creates an increase in this ratio immediately above the canopy. Although vegetation height in screenhouses is usually low, the fetch requirement becomes large and may lead to underestimation of the EC-measured flux. How the footprint model may be used for estimating the ratio between the EC measured flux and the depth-integrated sources is illustrated provided the fluxes from outside the screenhouse are known (or negligible). This illustration is carried out in typical banana screenhouses, where EC measurements were available, showing reasonable skill in predicting the flux ratio as measured by two EC flux sensors positioned at two different heights and for two scalars (CO_2 and H_2O) that differ in their source–sink distribution inside the canopy.

Acknowledgments This work was supported by Research Grant Award No. IS-4374-11C from BARD, the United States–Israel Binational Agricultural Research and Development Fund.

References

Baldocchi D (1997) Flux footprints within and over forest canopies. Boundary-Layer Meteorol 85(2):273–292

Borgas MS, Flesch TK, Sawford BL (1997) Turbulent dispersion with broken reflectional symmetry. J Fluid Mech 332:141–156

Dicken U (2011) Eddy covariance measurements of turbulent fluxes in large agricultural screenhouses. PhD Thesis, The Hebrew University of Jerusalem, Israel, 78 pp

Dicken U, Cohen S, Tanny J (2013) Effect of plant development on turbulent fluxes of a screenhouse banana plantation. Irrig Sci 31(4):701–713

Finnigan J (2000) Turbulence in plant canopies. Annu Rev Fluid Mech 32:519–571

Horst T, Weil J (1992) Footprint estimation for scalar flux measurements in the atmospheric surface layer. Boundary-Layer Meteorol 59(3):279–296

Hsieh CI, Katul GG (2009) The Lagrangian stochastic model for estimating footprint and water vapor fluxes over inhomogeneous surfaces. Int J Bioclimatol Biometeorol 53(1):87–100

Hsieh CI, Katul GG, Schieldge J, Sigmon JT, Knoerr KK (1997) The Lagrangian stochastic model for fetch and latent heat flux estimation above uniform and nonuniform terrain. Water Resour Res 33(3):427–438
Hsieh C, Katul GG, Chi T (2000) An approximate analytical model for footprint estimation of scalar fluxes in thermally stratified atmospheric flows. Adv Water Resour 23(7):765–772
Hsieh CI, Siqueira M, Katul GG, Chu CR (2003) Predicting scalar source–sink and flux distributions within a forest canopy using a 2-D Lagrangian stochastic dispersion model. Boundary-Layer Meteorol 109(2):113–138
Kurbanmuradov O, Sabelfeld K (2000) Lagrangian stochastic models for turbulent dispersion in the atmospheric boundary layer. Boundary-Layer Meteorol 97(2):191–218
Leclerc M, Thurtell G (1990) Footprint prediction of scalar fluxes using a markovian analysis. Boundary-Layer Meteorol 52(3):247–258
Lee X (2003) Fetch and footprint of turbulent fluxes over vegetative stands with elevated sources. Boundary-Layer Meteorol 107(3):561–579
Li P, Taylor P (2005) Three-dimensional Lagrangian simulation of suspended particles in the neutrally stratified atmospheric surface layer. Boundary-Layer Meteorol 116(2):301–311
Mao S, Leclerc MY, Michaelides EE (2008) Passive scalar flux footprint analysis over horizontally inhomogeneous plant canopy using large-eddy simulation. Atmos Environ 42(21):5446–5458
Markkanen T, Rannik Ü, Marcolla B, Cescatti A, Vesala T (2003) Footprints and fetches for fluxes over forest canopies with varying structure and density. Boundary-Layer Meteorol 106(3):437–459
Möller M, Tanny J, Li Y, Cohen S (2004) Measuring and predicting evapotranspiration in an insect-proof screenhouse. Agric For Meteorol 127(1):35–51
Pasquill F (1971) Atmospheric dispersion of pollution. Q J R Meteorol Soc 7(414):369–395
Pasquill F (1972) Some aspects of boundary layer description. Q J R Meteorol Soc 98(417):469–494
Poggi D, Katul GG, Cassiani M (2008) On the anomalous behavior of the Lagrangian structure function similarity constant inside dense canopies. Atmos Environ 42(18):4212–4231
Prabha T, Leclerc M, Baldocchi D (2008) Comparison of in-canopy flux footprints between large-eddy simulation and the Lagrangian simulation. J Appl Meteorol 47(8):2115–2128
Rannik Ü, Aubinet M, Kurbanmuradov O, Sabelfeld K, Markkanen T, Vesala T (2000) Footprint analysis for measurements over a heterogeneous forest. Boundary-Layer Meteorol 97(1):137–166
Rannik Ü, Markkanen T, Raittila J, Hari P, Vesala T (2003) Turbulence statistics inside and over forest: influence on footprint prediction. Boundary-Layer Meteorol 109(2):163–189
Rannik Ü, Sogachev A, Foken T, Göckede M, Kljun N, Leclerc (2012) Footprint analysis, Springer, Berlin, pp 211–261
Reynolds A (1998a) On the formulation of Lagrangian stochastic models of scalar dispersion within plant canopies. Boundary-Layer Meteorol 86(2):333–344
Reynolds A (1998b) On trajectory curvature as a selection criterion for valid Lagrangian stochastic dispersion models. Boundary-Layer Meteorol 88(1):77–86
Rodean H (1996) Stochastic Lagrangian models of turbulent diffusion. Meteorological Monographs, vol 26(48). American Meteorological Society, Boston, 84 pp
Sawford B (1999) Rotation of trajectories in Lagrangian stochastic models of turbulent dispersion. Boundary-Layer Meteorol 93(3):411–424
Schmid HP (2002) Footprint modeling for vegetation atmosphere exchange studies: a review and perspective. Agric For Meteorol 113(1):159–183
Siqueira M, Katul GG, Tanny J (2012) The effect of the screen on the mass, momentum, and energy exchange rates of a uniform crop situated in an extensive screenhouse. Boundary-Layer Meteorol 142(3):339–363
Sogachev A, Lloyd J (2004) Using a one-and-a-half order closure model of the atmospheric boundary layer for surface flux footprint estimation. Boundary-Layer Meteorol 112(3):467–502
Sogachev A, Leclerc MY, Karipot A, Zhang G, Vesala T (2005) Effect of clearcuts on footprints and flux measurements above a forest canopy. Agric For Meteorol 133(1):182–196
Steinfeld G, Raasch S, Markkanen T (2008) Footprints in homogeneously and heterogeneously driven boundary layers derived from a Lagrangian stochastic particle model embedded into large-eddy simulation. Boundary-Layer Meteorol 129(2):225–248
Tanny J (2013) Microclimate and evapotranspiration of crops covered by agricultural screens: a review. Biosyst Eng 114(1):26–43
Tanny J, Haijun L, Cohen S (2006) Airflow characteristics, energy balance and eddy covariance measurements in a banana screenhouse. Agric For Meteorol 139(1):105–118
Tanny J, Dicken U, Cohen S (2010) Vertical variation in turbulence statistics and energy balance in a banana screenhouse. Biosyst Eng 106(2):175–187
Thomson D (1987) Criteria for the selection of stochastic models of particle trajectories in turbulent flows. J Fluid Mech 180:529–556

Vesala T, Rannik Ü, Leclerc M, Foken T, Sabelfeld K (2004) Flux and concentration footprints. Agric For Meteorol 127(34):111–116

Vesala T, Kljun N, Rannik U, Rinne J, Sogachev A, Markkanen T, Sabelfeld K, Foken T, Leclerc M (2008) Flux and concentration footprint modelling: state of the art. Environ Pollut 152(3):653–666

Wilson JD, Flesch TK (1997) Trajectory curvature as a selection criterion for valid Lagrangian stochastic dispersion models. Boundary-Layer Meteorol 84(3):411–425

Wilson J, Thurtell G, Kidd G (1981) Numerical simulation of particle trajectories in inhomogeneous turbulence, II: systems with variable turbulent velocity scale. Boundary-Layer Meteorol 21(4):423–441